

Constraints on the Near-Distance Saturation of Ground-Motion Amplitudes for Small-to-Moderate Induced Earthquakes

by Gail M. Atkinson, Emrah Yenier, Nitin Sharma, and Vincenzo Convertito

Abstract The accurate modeling of ground motion for induced-seismicity hazard estimation is critically dependent on how amplitudes scale with distance near the hypocenter. A rich database of ground motions from small events recorded at close distances in the Geysers region of California has been used to constrain the near-distance saturation effects that control the maximum observed ground motions and intensities for shallow-induced events. The results of this study support the modeling of these effects using an equivalent point-source concept, in which the effective source depth increases from a value near 1 km at moment magnitude (M) of 2 to a value near 3 km at M 4. This near-distance saturation behavior can be applied to the development of ground-motion models for induced seismicity in any region.

Introduction

A key question for the modeling of ground motion for induced-seismicity hazard estimation concerns how amplitudes scale with distance near the hypocenter. Traditional databases for the development of ground-motion prediction equations (GMPEs) tend to be very sparse at short hypocentral distances, partly because ground-motion observations are sparse in general at close distances due to seismic network configuration and partly because typical depths of most earthquakes (≥ 5 km) limit the hypocentral distance range that can be observed. For example, the Next Generation Attenuation (NGA)-West2 database for crustal earthquakes in active tectonic regions (Ancheta *et al.*, 2014) is rich in observations over a wide range of magnitudes and distances but contains limited information to constrain the scaling of ground-motion amplitudes within 5 km of the hypocenter. This scaling behavior is critical for the development of GMPEs for induced-seismicity applications, for which much of the hazard is likely concentrated at sites in close proximity to the hypocenter (e.g., Convertito *et al.*, 2012; Hough, 2014).

Atkinson (2015) used the NGA-West2 database to develop an empirical GMPE for small-to-moderate events at close distances, for use in induced-seismicity applications, under the assumption that shallow natural events and induced events should have similar ground motions for equivalent hypocentral distances. However, the limitations of the database resulted in a wide uncertainty band for median motions for events of moment magnitude (M) 3–5 at distances within about 5 km of the epicenter. This uncertainty is critical to conclusions concerning the damage potential of small shallow events that may be induced by nearby field operations (Atkinson *et al.*, 2015).

Yenier and Atkinson (2015b) used an equivalent point-source model to develop and calibrate GMPEs for both natu-

ral and induced events in central and eastern North America (CENA). They showed that the source parameter controlling high-frequency ground motion (the stress parameter) is a strong function of focal depth, but no significant dependence on whether an event is natural or induced was evident. Using the framework of the equivalent point-source model, robust and transportable GMPEs can be developed for both western and eastern environments in North America, for either natural or induced events (Yenier and Atkinson, 2014, 2015a,b). However, a key parameter to constrain such GMPE models is the shape of the near-distance saturation function. Typically, this function takes a form that is equivalent to an added focal depth term, with the added depth term being an increasing function of magnitude (e.g., Atkinson and Silva, 2000; Yenier and Atkinson, 2014). The attenuation is framed in terms of an equivalent point source at an effective distance of R , given by

$$R = \sqrt{r^2 + h_{\text{eff}}^2}, \quad (1)$$

in which r is the rupture distance or, for small events, distance to the hypocenter ($r \approx R_{\text{hypo}}$), and h_{eff} is the effective depth term that controls near-distance saturation. It is h_{eff} that causes the attenuation curve to approach a constant amplitude as the hypocenter (or fault plane) is approached. This term is a function of magnitude, becoming larger as magnitude increases. In Figure 1, the concept is illustrated using data from the NGA-West2 database to show typical saturation effects that have been observed. The effective-depth function has been empirically constrained for large ($M > 6$) earthquakes in previous studies (e.g., Atkinson and Silva, 2000; Yenier and Atkinson, 2014), but has been inherently difficult to constrain for smaller events, due to the paucity of data at sufficiently short hypocentral distances. For example, Yenier and Atkinson (2015b), in

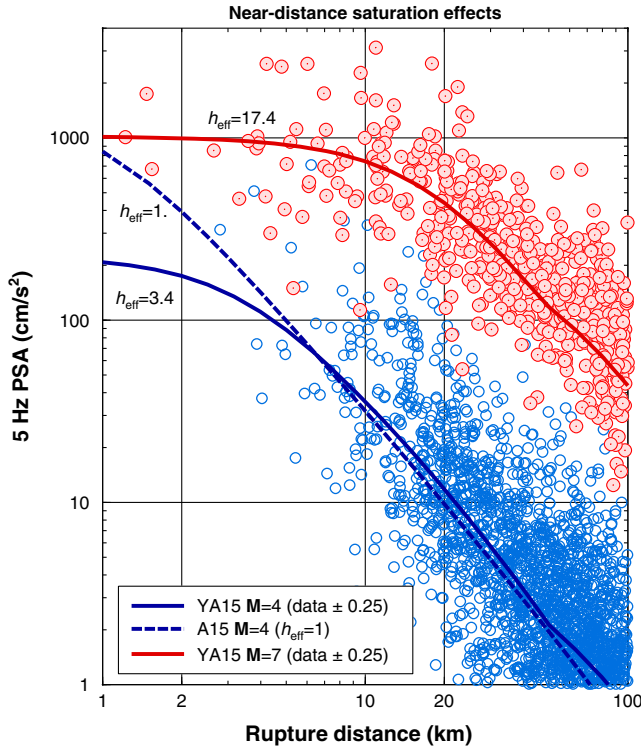


Figure 1. Illustration of the effect of h_{eff} on ground-motion attenuation at short distances. The solid ground-motion prediction equation (GMPE) curves are for the California equivalent point-source GMPE as given in Yenier and Atkinson (2015b; hereafter, YA15), for B/C site conditions for M 4 ($h_{\text{eff}} = 3.4$ km) and M 7 ($h_{\text{eff}} = 17.4$ km). The dashed line shows Atkinson (2015; hereafter, A15) empirical small- M GMPE for California (B/C site conditions) for M 4 (for the initial assumed form with $h_{\text{eff}} = 1$ km). Data from the Next Generation Attenuation (NGA)-West2 database, for events within 0.25 M units of the selected magnitudes, corrected to B/C site conditions using the site factors of Boore *et al.* (2014), are plotted for comparison. Note the paucity of data to constrain the shape for M 4. PSA, pseudospectral acceleration. The color version of this figure is available only in the electronic edition.

their GMPE development for CENA (and western North America [WNA]), used an effective depth term given as follows:

$$h_{\text{eff}} = 10^{-0.405+0.235M}. \quad (2)$$

This relation was defined using ground-motion amplitude data that constrain the near-distance saturation for events of $M > 6$ (Atkinson and Silva, 2000; Yenier and Atkinson, 2014), but the extension of the trend to events of $M < 6$ was an informed guess, based on the concept that the effective depth should approach small values for small events ($M < \sim 4$), and based on a practical consideration; specifically, if h_{eff} scales too steeply at lower magnitudes, it results in GMPE curves that cross each other at very close distances. The ambiguity in defining this near-hypocentral shape is important in both empirical and model-based GMPEs. For example, in the strictly empirical GMPE model of Atkinson (2015) for small-to-moderate events at close distances, the functional form also included an effective depth term. This term was initially assumed to approach $h_{\text{eff}} =$

1 km for $M \leq 4$, but an alternative form in which $h_{\text{eff}} = 3$ km at M 4 (similar to the Yenier and Atkinson, 2015b, model) was also considered. As shown in Figure 1, these two alternative values for h_{eff} at M 4 have very different implications for near-source motions for M 4 events.

In this study, we examine the near-distance scaling of small events at close distances, using a rich database of ground motions from small ($M < 4$) induced events, recorded in the Geysers geothermal region of California, at hypocentral distances < 20 km. The database is described by Sharma *et al.* (2013) and is used here without any further filtering or modification. It comprises three-component records of 5% damped pseudospectral acceleration (PSA) at 0.2, 0.5, and 1 s, and peak ground acceleration (PGA) and peak ground velocity (PGV); in total, there are 5450 records within 20 km of the hypocenter, from 212 shallow events (0.5–3 km in depth) of M 1.5–3.6. The site conditions of the recordings are not known, but the region is believed to be characterized as the National Earthquake Hazards Reduction Program class C (NEHRP C; near-surface shear-wave velocities of 360–760 m/s) (Sharma *et al.*, 2013). All of the events were recorded at 10 or more stations, and all stations recorded multiple events, providing an excellent database in magnitude–distance space for the use of empirical techniques to distinguish source, path, and site effects (e.g., see Fig. 2 for magnitude–distance distribution). This allows the robust determination of the effective depth parameter for events of M 1.5–3.6.

Study Methods

Determination of Moment Magnitude

The first step of the analysis is to determine the moment magnitude M of all of the study events. This is done using the method of Atkinson *et al.* (2014), as refined by Novakovic and Atkinson (2015). The algorithm is based on using the vertical-component PSA amplitudes at 1 s for events of $M > 3$ and the PSA amplitudes at 0.3 s for events of $M < 3$. It has been shown that for small events the response spectrum at these periods is controlled by seismic moment, allowing robust estimates of M . The vertical component is used in the algorithm to minimize the effects of site response. Nevertheless, significant site-response effects are often observed on the vertical component, and thus it is desirable to account for site terms when possible. This is easily done in this study because the stations recorded many events, enabling robust site terms to be calculated empirically using residual analysis. We proceed as follows: we first estimate M as described by Atkinson *et al.* (2014), using the WNA formula; then, the M values corresponding to both the 1 s and the 0.3 s PSA values are calculated for each event at each station. Note that to obtain the PSA value at 0.3 s, we interpolate (in log–log space) between the 0.2 and 0.5 s values of PSA that are provided in the database. The residuals for the M estimate, calculated relative to the average M for the event over all stations, are averaged by station to obtain a magnitude-correction site

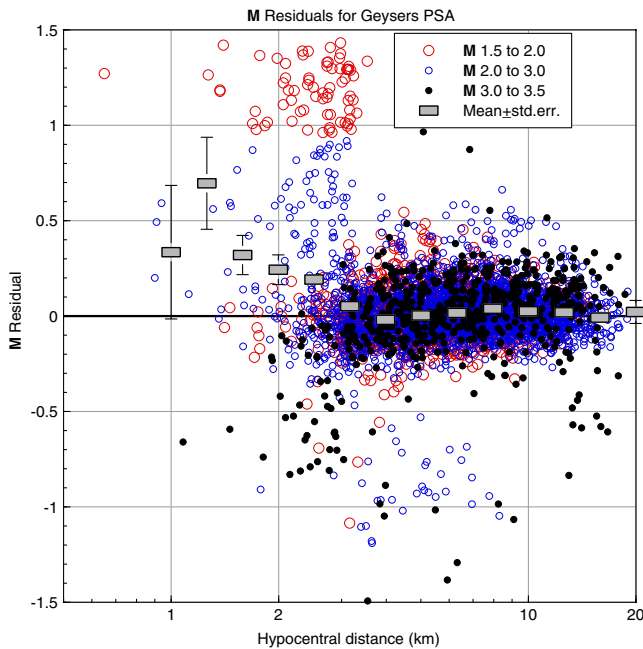


Figure 2. Residuals of the calculated value of M , from the second-pass estimation (after removal of average vertical-component site term at each station). Mean residuals and their standard errors in log-distance bins are also shown. The color version of this figure is available only in the electronic edition.

term for each station (for 1 and 0.3 s). This correction term applies to the magnitude calculated at that station, and thus applies to the vertical component, with a separate site term being calculated for 1 and 0.3 s. It is a correction term that expresses whether the magnitude estimated at that site is systematically high or low relative to the event magnitude as averaged over all stations. Thus, the average of these magnitude correction terms over all stations will be zero.

The site terms are then applied in a second-pass calculation of M . In the second pass, the site-term-corrected values of M from PSA at 1 and 0.3 s are calculated and combined as recommended by Novakovic and Atkinson (2015). Specifically, if the calculated value of M is > 3.0 for both the 1 and 0.3 s values of PSA, then the M calculated from the 1 s site-corrected PSA values is used. If the calculated value of M is < 3.0 for both the 1 and 0.3 s values, then the 0.3 s value of M is used. If neither of these conditions is satisfied, the average of the two M values is used.

Figure 2 shows the residuals for the M calculation as a function of distance and magnitude (from the second-pass determination of M). The mean residual is 0.02 with a standard deviation of 0.22 M units. The residuals are free of any apparent trends, suggesting that the model is producing stable M estimates. We noted that the residuals for the initial M calculation, before applying the site-correction factors (not plotted), were distributed similarly but had larger scatter, as would be expected. Moreover, the M values obtained for each event are not noticeably affected by the second pass;

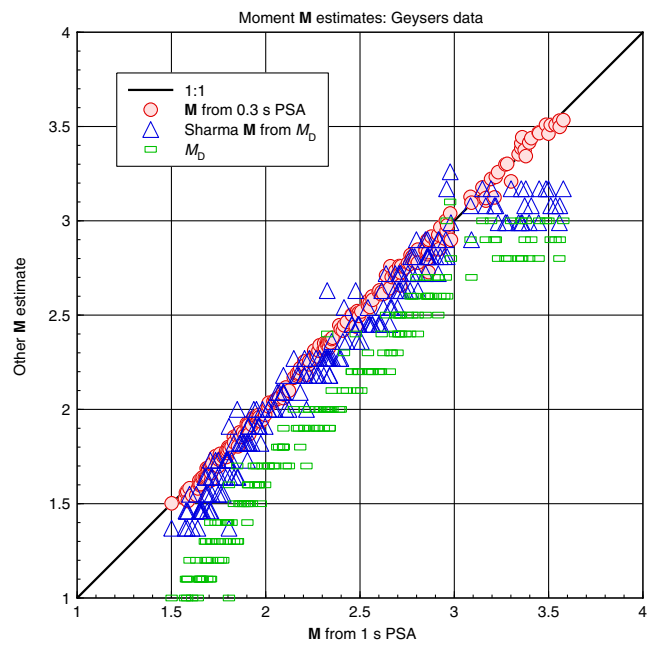


Figure 3. Estimated M from PSA at 0.3 s, and from duration magnitude (M_D) as given in Sharma *et al.* (2013), in comparison to values of M obtained from 1 s PSA. (Original M_D values before conversion are also shown.) The color version of this figure is available only in the electronic edition.

thus, the main advantage of removing the site terms is to reduce the between-station scatter in the magnitude estimates.

It is interesting that the residuals scatter greatly at very close distances, with small events exhibiting some very high residuals at the closest distances, and larger events showing lower residuals at close distances. This is indicative of saturation effects in the near-source amplitudes that we are aiming to model with the h_{eff} term. We note that there is no saturation term in the M calculation formula, as it is generally expected that most stations from which M is to be determined will be beyond the distance range where h_{eff} is important. By finding the appropriate h_{eff} value for each event in this study, we should be able to reduce this near-distance scatter. Although we are modeling the near-distance scatter as being primarily due to saturation effects, we acknowledge that some of it may be attributable to location error, especially for the smallest events. Moreover, there may be other source effects for some small events, as evident by the cluster of high residuals (even after removing site terms) for events of M 1.5–2.0; such effects might include radiation pattern or directivity effects, for example.

The estimates of M that were obtained from PSA at 1 and 0.3 s were mutually consistent. This is shown in Figure 3, which plots the estimated value of M from the 0.3 s PSA in comparison to that from the 1 s PSA. The estimated values of M that were obtained by Sharma *et al.* (2013) using an empirical conversion from duration magnitude (M_D) are also shown, along with the original M_D estimates used to characterize the events. The M estimates from this study are generally

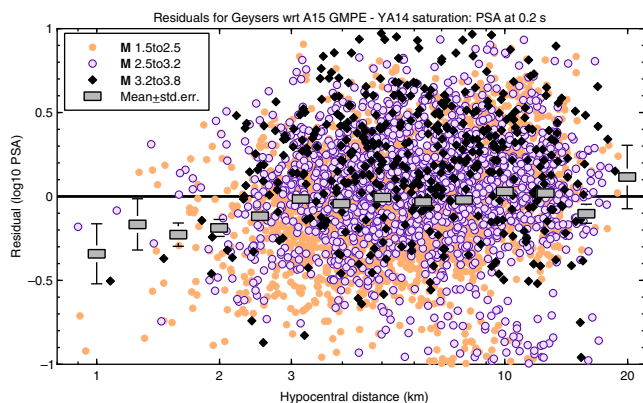


Figure 4. Residuals for the Geysers horizontal-component ground-motion observations (on C sites) with respect to the A15 GMPE (for B/C sites): PSA at 0.2 s. Mean residuals and their standard errors in log–distance bins are also shown. The color version of this figure is available only in the electronic edition.

larger than those estimated by [Sharma *et al.* \(2013\)](#) using M_D ; the differences are small (~ 0.1 – 0.2 units) for M 2–3 events, but somewhat larger at lower and higher magnitudes. This is not surprising, if we consider that duration is difficult to measure for small events, and that M_D may saturate rapidly as magnitude increases.

Calculation of Horizontal-Component Site Terms for Each Station

An important component of empirical analyses to examine attenuation behavior is the separation of source, path, and site effects. With the value of M determined for each event, we turn our attention to the analysis of path and site effects in the horizontal-component ground-motion data. We use the geometric mean of the two horizontal components, which is equivalent on average to the horizontal-component measure used in the NGA-West2 database. We begin by comparing the Geysers observations to the predictions of the empirical GMPE of [Atkinson \(2015; hereafter, A15\)](#), which was developed from close-distance PSA observations of California earthquakes of M 3–6, adjusted for site effects so as to be applicable for sites at the B/C boundary (760 m/s); this is a subset of the NGA-West2 database used by [Boore *et al.* \(2014\)](#). We note that this comparison is a significant extrapolation of the A15 equation beyond its applicable data range when applied to events as small as M 1.5. Moreover, the Geysers sites are believed to be NEHRP C sites, and thus there may be significant amplification relative to the California model for B/C, at least at some sites. In Figures 4 and 5, we plot the residuals for the Geysers data (without any site corrections) in comparison to the A15 GMPE (for B/C sites), for 0.2 and 1 s, respectively. We used the [Yenier and Atkinson \(2014\)](#) saturation form of the A15 GMPE, as shown in Figure 1 (rather than the alternative saturation model). A check revealed that the average residuals by station (i.e., the calculated site terms) are not sensitive to this choice. How-

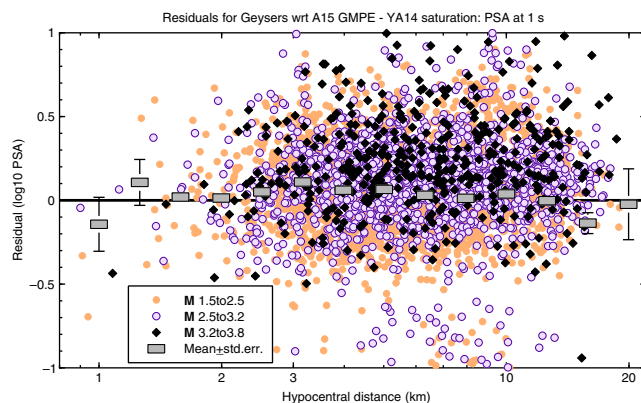


Figure 5. Residuals for the Geysers horizontal-component ground-motion observations (on C sites) with respect to the A15 GMPE (for B/C sites): PSA at 1 s. Mean residuals and their standard errors in log–distance bins are also shown. The color version of this figure is available only in the electronic edition.

ever, residuals at very close distances may be affected. In particular, although there are no residual trends at distances beyond about 3 km, we note in Figure 4 that the 0.2 s residuals are negative at very close distances, suggesting that there may be more pronounced near-distance saturation than is assumed in the [Yenier and Atkinson \(2014\)](#) saturation function. A refinement of this saturation is what will be accomplished in the [Determination of Effective Depth Term](#) section.

Overall, the Geysers horizontal-component PSA values are consistent with the A15 model, even for magnitudes as small as $M \sim 2$. The noted residual trends can be attributed to the NEHRP C site conditions that prevail in the Geysers region, in comparison to the reference B/C site condition for the A15 GMPE, and to the near-distance saturation effects that we intend to model in the following. Therefore, we conclude that a reasonable estimate of the site amplification for each station may be obtained as the average residual with respect to the A15 GMPE. Our motivation in using the average station residuals relative to A15 as a site-response estimate is that we lack a viable alternative. There are no obvious reference sites available; all stations are believed to be on NEHRP C or similar, but with unknown profiles.

We implicitly assumed that site response is linear, as we have not considered amplitude dependence of the site term. This is likely a reasonable approximation for the bulk of the observations in this study (which have $PGA < 5\%$), though it is possible that nonlinearity could reduce amplitudes for a few of the larger events at high frequencies for very close distances. We also assume that any source effects in the residuals, such as those due to differences in the stress parameter from one event to another, will average out when the residuals at each site are averaged over multiple events. We acknowledge that any systematic difference in source levels between the Geysers and the NGA-W2 events will map into the site terms. However, these effects are expected to be minimal, because for events of this size the motions are controlled by the seismic moment for most of the period band considered here. The

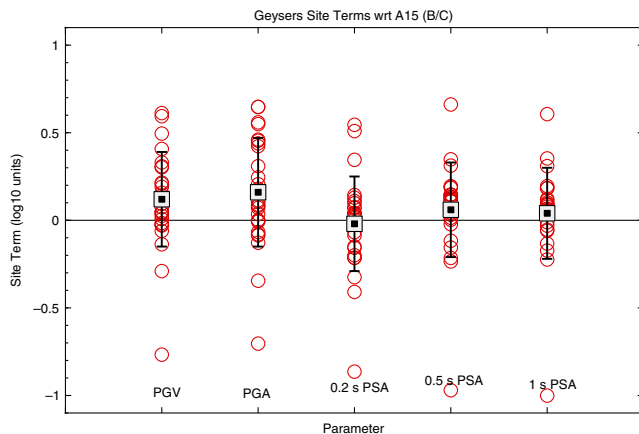


Figure 6. Site terms inferred for the Geysers stations, based on averaging residuals with respect to the A15 GMPE by station. Circles show values obtained for each station, squares with error bars are mean and standard deviation for each ground-motion parameter (peak ground velocity [PGV], peak ground acceleration [PGA], and PSA at 0.2, 0.5, and 1 s). The x axis is an arbitrary ordering of the five plotted parameters. The color version of this figure is available only in the electronic edition.

interperiod stability of the site terms, as shown in the following, supports this expectation.

Figure 6 shows the behavior of the inferred site amplification terms, taken as the average difference between the observations at each site and the A15 GMPE. By subtracting the average site term for each station from the observations, we reduce the station-to-station variability in the observed horizontal-component PSA values, and obtain the inferred equivalent values for B/C site conditions. The site terms are significant for some stations, but the average value over all stations is near zero for PSA at 0.2, 0.5, and 1 s. There is a positive residual of 0.1–0.2 \log_{10} units (average amplification by a factor of 1.2–1.5) for PGA and PGV.

Determination of Effective Depth Term

The site-corrected horizontal-component Geysers observations are used to find the most effective depth value that expresses the near-distance attenuation shape, on an event-by-event basis. We isolate this term from the overall attenuation using the equivalent point-source model of Yenier and Atkinson (2015b). Specifically, the attenuation function for response spectra, considering geometrical spreading and near-distance saturation, is given by

$$FZ = \ln(Z) + (b_3 + b_4 \mathbf{M}) \ln(R/R_{\text{ref}}), \quad (3)$$

in which the effective distance (R) is as defined in equation (1) and R_{ref} is the reference effective distance, given as $R_{\text{ref}} = \sqrt{r^2 + h_{\text{eff}}^2}$. The first term in equation (3) expresses the geometric spreading term given by $Z = R^{-1.3}$ for distances < 50 km in California (Yenier and Atkinson, 2015a). The second term represents the magnitude dependence that results from the nonstationary response of an oscillator (the

difference between attenuation in the Fourier and response spectral domains), in which b_3 and b_4 are coefficients given in Yenier and Atkinson (2015b). We consider hypocentral distance to be equivalent to fault-rupture distance for events of $\mathbf{M} < 4$, which includes all of the events in the Geysers dataset.

The attenuation function of equation (3), as based on an equivalent point-source stochastic model, is consistent with that found empirically in Atkinson (2015), for events of \mathbf{M} 3–5, even though the functional form appears quite different. For example, the application of equation (3) gives an equivalent attenuation slope for PGA from 10 to 40 km of $R^{-1.74}$ for \mathbf{M} 3, whereas the A15 GMPE rate is equivalent to $R^{-1.75}$. The consistency of attenuation rates can also be seen in Figure 1.

The attenuation-corrected amplitude at the source for event i at station j can be expressed as follows:

$$E_{ij} = \ln Y_{ij} - FZ - \chi(R_{\text{hypo}}), \quad (4)$$

in which Y_{ij} is the site-corrected ground-motion observation from event i at station j , FZ is given by equation (3), and χ is the frequency-dependent anelastic-attenuation coefficient from Yenier and Atkinson (2015b) for California. For a specified value of h_{eff} , we can obtain the average source amplitude, E_i (in \ln units) by averaging E_{ij} over all stations. The standard deviation of E_i will be minimized by choosing a value of h_{eff} that best expresses the attenuation shape for the event. We find this value by evaluating the source terms and their error for values of h_{eff} from 0.1 to 10 km. Keep in mind that h_{eff} is an attenuation shape parameter that is not necessarily related to the actual focal depth of the events, which are all quite shallow (< 3 km).

Values obtained for h_{eff} that minimize the error in the attenuation model of equation (4) are plotted in Figure 7, using for each event the average value obtained over the five ground-motion parameters (PSA at 0.2, 0.5, and 1 s, PGA, and PGV). We chose the average value after noting that the behavior of h_{eff} for each of the ground-motion parameters, when considered individually, is the same as that for the average taken over all five. The values of h_{eff} scatter, mostly between 0 and 4 km, with a weak but statistically significant trend in \mathbf{M} . The trend is more apparent when the mean value of h_{eff} is calculated in magnitude bins (0.5 units in width). We conclude that h_{eff} has a value near 1 km for $\mathbf{M} < 2$, increasing to a value near 2 km for \mathbf{M} 2.5–3.5. We infer from the trend that the average value of h_{eff} for $\mathbf{M} \sim 4$ should be near 3 km; this is in agreement with the alternative saturation model considered in Atkinson (2015), and the model used for the CENA GMPE by Yenier and Atkinson (2015b). However, it is noteworthy that the scatter in values implies that near-distance saturation effects are more apparent in some events than in others. Moreover, the scatter appears particularly pronounced for the larger events, implying that near-distance saturation will not be uniformly observed for all events. Thus, for individual events, there is a significant potential

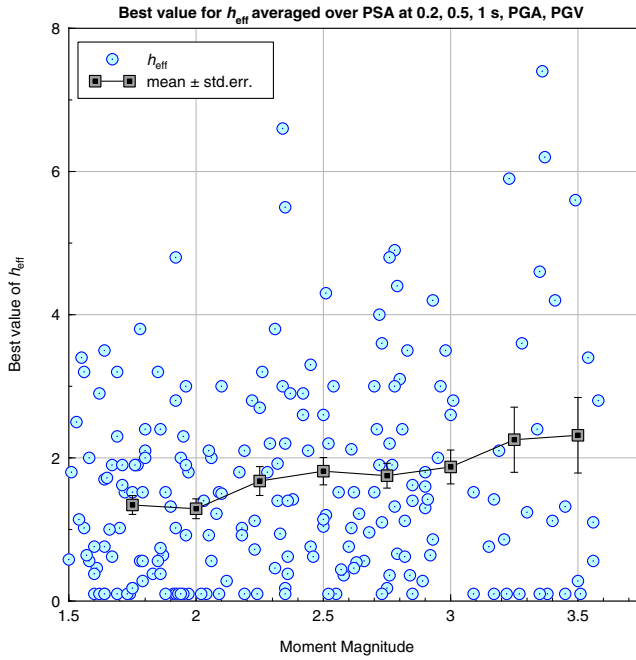


Figure 7. Best-fit values of h_{eff} obtained for the Geysers data. Circles show individual event values (averaged over PSA at 0.2, 0.5, and 1 s, PGA, and PGV). Squares show average values in overlapping 0.5 magnitude unit bins, with error bars representing the standard error of the mean. The color version of this figure is available only in the electronic edition.

for motions that are larger (or smaller) than median values expected based on this saturation function.

It is useful to repeat the analysis conducted for the Geysers data for the NGA-West2 database used in the A15 GMPE. In that study, the near-distance saturation term was assumed, rather than determined, using two possible choices. Part of the reason for that approach was that there were not many events in the NGA-West2 database having sufficient near-distance observations to provide useful constraints on h_{eff} . This problem is exacerbated by the fact that some of the events in the NGA-West2 database are quite deep (> 10 km), and thus there are no observations possible at short hypocentral distances. Nevertheless, by repeating the analysis for the shallow events in the NGA-West2 database, we can extend the information at least a little toward larger magnitudes, as shown in Figure 8. In this plot, the error bars show standard deviation from the average values of h_{eff} (rather than standard error, which was shown in Fig. 7). The model line that was assumed by Yenier and Atkinson (2015b) in developing a GMPE for CENA (equation 2) is also plotted in Figure 8, and agrees well with both the Geysers and shallow (< 8 km deep) NGA-West2 events.

Discussion and Conclusions

The source terms (E_i) for the events plotted in Figure 8 can be used to examine the expected median ground-motion amplitudes at the epicenter, as a function of magnitude (using

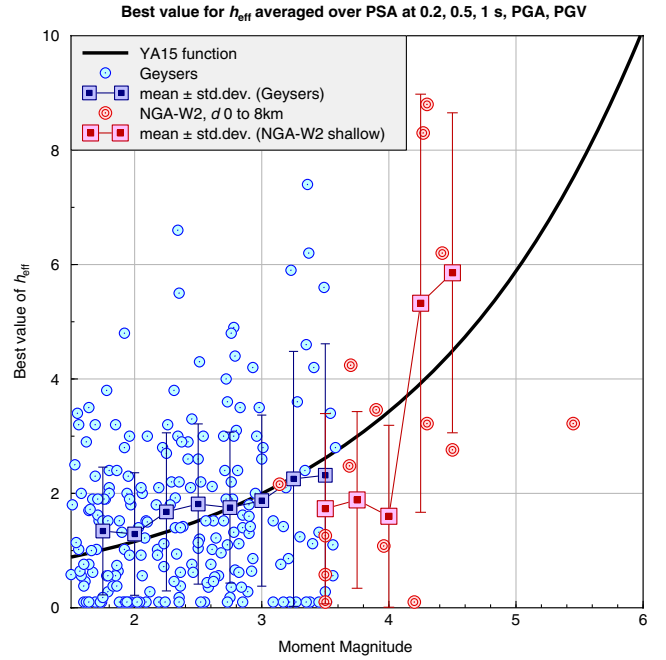


Figure 8. Best-fit values of h_{eff} obtained for the Geysers data, in comparison to corresponding values for events in the NGA-West2 database. Circles show individual event values (averaged over PSA at 0.2, 0.5, and 1 s, PGA, and PGV). Squares show average values in overlapping magnitude bins 0.5 units in width (all events for the Geysers, events with depth (d) 0–8 km for NGA-West2), with error bars representing the standard deviation of the mean. Plotted line is for equation (2). The color version of this figure is available only in the electronic edition.

the obtained value of h_{eff} for each event). This allows us to examine the implications of the near-distance saturation shape and its variability on the median ground motions that might be expected above the hypocenter, at very close distances to the epicenter. To do this, we re-arrange the expression for the ground-motion amplitude (equation 4) to find the average event amplitude (Y_i) at an effective distance R that corresponds to $R_{\text{hypo}} = d$ (in which d is the focal depth).

Thus, we evaluate the expression for $R = \sqrt{h_{\text{eff}}^2 + d^2}$; this is the effective point-source depth associated with zero epicentral distance. The average event amplitudes that we infer at the epicenter are plotted in Figure 9. For the NGA-West2 events, we include only those events with depths < 8 km (most are in the 4–8 km depth range); by comparison the Geysers events are shallower on average, with depths of 1.5–3 km. Note that the NGA-West2 events tend to have lower motions near the epicenter for a given M even though their ground-motion attributes are otherwise comparable to those for the Geysers events (i.e., when viewed as a function of hypocentral distance the Geysers and NGA-West2 motions are similar for equivalent site conditions). This provides an illustration of the importance of focal depth in controlling the maximum ground motions near the epicenter. Specifically, Figure 9 suggests that near the epicenter the range of median PGV values for an event of M 3.5 is about 1–4 cm/s

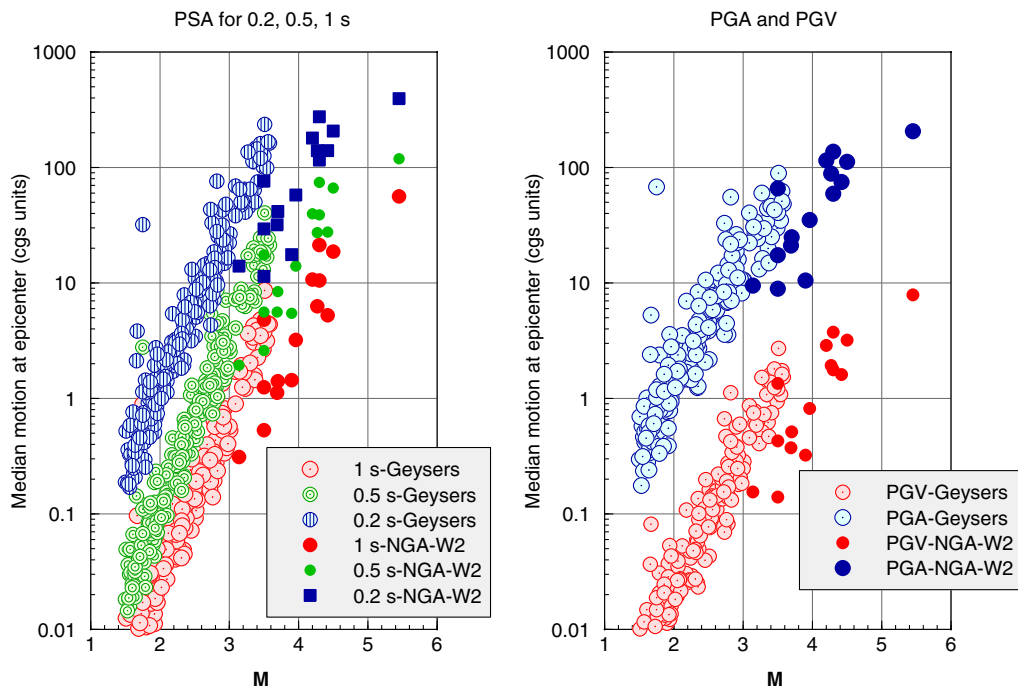


Figure 9. Median motions at zero epicentral distance for the Geysers and NGA-West2 events. NGA-West2 data are included for events with depth < 8 km (typical depths of 4–8 km). The Geysers events have depths of 1.5–3 km. The color version of this figure is available only in the electronic edition.

for the very shallow Geysers events. According to the correlations of Worden *et al.* (2012), this would imply a felt intensity of 4–5. In contrast, the deeper natural events in the NGA-West2 database (for events in the depth range from 4 to 8 km) have a range of median PGV values at the epicenter of about 0.2–0.8 cm/s for M 3.5, corresponding to epicentral intensities of 2.5–3.5. Note that if we considered PGA rather than PGV, we would infer higher intensities by ~ 0.5 to 1 unit in both cases. This result is in agreement with the observation made by Hough (2014), that induced events tend to have relatively high intensities at close distances (but not at larger distances).

In summary, a rich database of ground motions from small events recorded at close distances in the Geysers area of California has been used to constrain the near-distance saturation effects that control the maximum observed ground motions and intensities for shallow events. The results of this study support the modeling of these effects using an equivalent point-source concept, in which the effective depth is as given by equation (2) (from Yenier and Atkinson, 2015b). There is a significant event-to-event variability in the near-distance saturation term, such that the saturation effects for individual events may be stronger or weaker than that given by equation (2) by about a factor of 2 (standard deviation).

Data and Resources

The Geysers data were provided by the Geothermal Engineering Integration Mitigation of Induced Seismicity in Reservoirs (GEISER) project, whereas the Next Generation

Attenuation (NGA)-West2 database is available through the Pacific Engineering Research Center (<http://peer.berkeley.edu/>, last accessed January 2016). All figures were made using CoPlot (www.cohort.com, last accessed January 2016).

Acknowledgments

G. M. A. and E. Y. are supported by the Natural Sciences and Engineering Research Council of Canada. The Geysers database was provided by the Geothermal Engineering Integration Mitigation of Induced Seismicity in Reservoirs (GEISER) project. N. S. is thankful for the support received from the Lithosphere-Atmosphere-Ionosphere-Magnetosphere Coupling project funded by the Department of Science and Technology of India.

References

- Ancheta, T., R. Darragh, J. Stewart, E. Seyhan, W. Silva, B. Chiou, K. Wooddell, R. Graves, A. Kottke, D. Boore, *et al.* (2014). PEER NGAWest2 database, *Earthq. Spectra* **30**, 989–1006.
- Atkinson, G. (2015). Ground-motion prediction equation for small-to-moderate events at short hypocentral distances, with application to induced seismicity hazards, *Bull. Seismol. Soc. Am.* **105**, 981–992, doi: [10.1785/0120140142](https://doi.org/10.1785/0120140142).
- Atkinson, G., and W. Silva (2000). Stochastic modeling of California ground motions, *Bull. Seismol. Soc. Am.* **90**, 255–274.
- Atkinson, G., H. Ghofrani, and K. Assatourians (2015). Impact of induced seismicity on the evaluation of seismic hazard: Some preliminary considerations, *Seismol. Res. Lett.* **86**, 1009–1021.
- Atkinson, G., D. W. Greig, and E. Yenier (2014). Estimation of moment magnitude (M) for small events ($M < 4$) on local networks, *Seismol. Res. Lett.* **85**, 1116–1124.
- Boore, D., J. Stewart, E. Seyhan, and G. Atkinson (2014). NGA-West2 equations for predicting response spectral accelerations for shallow crustal earthquakes, *Earthq. Spectra* **30**, 1057–1086.

- Convertito, V., N. Maercklin, N. Sharma, and A. Zollo (2012). From induced seismicity to direct time-dependent seismic hazard, *Bull. Seismol. Soc. Am.* **102**, no. 6, 2563–2573, doi: [10.1785/0120120036](https://doi.org/10.1785/0120120036).
- Hough, S. (2014). Shaking from injection-induced earthquakes in the central and eastern United States, *Bull. Seismol. Soc. Am.* **104**, 2619–2626, doi: [10.1785/0120140099](https://doi.org/10.1785/0120140099).
- Novakovic, M., and G. Atkinson (2015). Preliminary evaluation of ground motions from earthquakes in Alberta, *Seismol. Res. Lett.* **86**, 1086–1095, doi: [10.1785/0220150059](https://doi.org/10.1785/0220150059).
- Sharma, N., V. Convertito, N. Maercklin, and A. Zollo (2013). Ground-motion prediction equations for the Geysers geothermal area based on induced seismicity records, *Bull. Seismol. Soc. Am.* **103**, 117–130.
- Worden, B., M. Gerstenberger, D. Rhoades, and D. Wald (2012). Probabilistic relationships between ground motion parameters and modified Mercalli intensity in California, *Bull. Seismol. Soc. Am.* **102**, 204–221.
- Yenier, E., and G. Atkinson (2014). Point-source modeling of moderate-to-large magnitude earthquakes and associated ground-motion saturation effects, *Bull. Seismol. Soc. Am.* **104**, 1458–1478.
- Yenier, E., and G. Atkinson (2015a). An equivalent point-source model for stochastic simulation of earthquake ground motions in California, *Bull. Seismol. Soc. Am.* **105**, 1435–1455.
- Yenier, E., and G. Atkinson (2015b). A regionally-adjustable generic GMPE based on stochastic point-source simulations, *Bull. Seismol. Soc. Am.* **105**, 1989–2009.

Department of Earth Sciences
Western University
London, Ontario
Canada N6A 5B7
gmatkinson@aol.com
(G.M.A., E.Y.)

Indian Institute of Geomagnetism
Plot 5, Sector 18, New Panvel
Navi Mumbai 410218, India
(N.S.)

Istituto Nazionale di Geofisica e Vulcanologia
via di Vigna Murata, 605
00143 Rome, Italy
(V.C.)

Manuscript received 6 March 2016;
Published Online 9 August 2016